Modeling the long-term evolution of dilute solid solutions in the presence of vacancy fluxes

Thomas Schuler,[1,2,*] Pascal Bellon,[1] Dallas R. Trinkle,[1] and Robert S. Averback[1]
[1]*Department of Materials Science and Engineering, University of Illinois, Urbana-Champaign, Illinois 61801, USA*
[2]*Université Lyon, IMT Mines Saint-Etienne, Centre SMS, LGF, F-42023 Saint-Etienne, France*

(Received 28 February 2018; published 16 July 2018)

This work investigates the long-term evolution of dilute solute atoms in face-centered-cubic (fcc) alloys driven by sustained vacancy fluxes, as for instance in the case of materials subjected to energetic particle irradiation. Employing the five-jump frequency framework, we provide compact analytic expressions of the Onsager matrix for dilute vacancy-solute systems in form of a ratio of polynomial functions of jump frequencies. The drag ratio is found to be a function of only two independent variables, which enables a systematic study of both the flux coupling and trapping behavior between solutes and point defects. Using an existing diffusivity database for a total of 182 solutes in 5 fcc solvents, we show that, while most vacancy-binding solutes have indeed a positive drag ratio, there are some solutes with positive, but small, or even negative drag ratio. This previously unnoticed feature is interesting as it would ensure that the trapping solute remains in the matrix despite the accumulation of irradiation dose. In the case where the drag ratio is positive, we propose a kinetic model of solute depletion over time due to flux coupling with vacancies and apply it to a Cu-1 at. % Sb alloy. This study reveals that solutes are not simply dragged to sinks by point defects, but affect the flux of point defects to sinks by modifying the transport coefficients and the driving force for point-defect elimination.

DOI: 10.1103/PhysRevMaterials.2.073605

I. INTRODUCTION

Materials' properties are generally controlled by thermomechanical treatments and chemical composition optimization. In the case of materials subjected to irradiation by energetic particles, for instance in nuclear reactors, alloy compositions are carefully chosen to ensure, as much as possible, that these materials retain their properties despite the damage introduced by irradiation. For instance, small amounts of solutes can be added to a matrix to trap point defect [1,2], without affecting much the bulk properties of the material. A potential issue, however, is that a high solute-defect binding energy is required to create strong traps, and it is therefore likely that the added solute will eventually migrate along with the defect [3], a phenomenon known as flux coupling [4–6]. There are many situations where flux coupling plays an important role, both on the kinetics and steady state of the system, such as quenching [4,7,8], irradiation [5,6,9,10], ball-milling, severe plastic deformation, carburization, surface oxidation, etc. This flux coupling could result in a gradual loss of solute to point-defect sinks, and thus in a progressive degradation of the materials properties. Hence, accurate and efficient modeling tools are needed to take flux coupling effects into account at the alloy design stage.

Theoretical developments over the last decade [11–13] combined with the increasing capacities of *ab initio* calculations make it now possible to compute flux coupling coefficients between solutes and point defects from atomic-scale processes in a wide range of materials [14–23], while older models [24,25] are still widely used by the community because of the small number of input parameters they require [26–34]. The difficulty in using these methods more systematically lies in the inherent complexity of the problem: while it is possible to directly compute transport coefficients for a given alloy system and a given composition, these calculations are computationally demanding. It is challenging to obtain these properties for a broad range of alloy systems, thus making it problematic to consider and compare many alloy systems. Materials' design would greatly benefit from simplified tools that rely on a small subset of alloy data. These tools, in conjunction with high-throughput calculations of atomic-scale properties, would then allow for an efficient screening across possible alloying elements before performing more accurate calculations.

The aim of this paper is to introduce one such practical tool for systematic investigation of solute diffusion in face-centered-cubic (fcc) solvents. The problem of vacancy-mediated diffusion of substitutional solutes in the face-centered-cubic lattice was first addressed with the five-frequency model which is essentially a first-nearest-neighbor approximation of vacancy-mediated solute diffusivity [35,36]. The full expression for transport coefficients was obtained later on using linear response theory [37] and then the so-called self-consistent mean field (SCMF) method [12]. Building on the latter, Garnier *et al.* [16] proposed a complete analysis of the drag ratio for Ni-Si systems in a so-called 3NN3NN approximation of the SCMF method. This approximation, which considers solutes up to the third-nearest neighbors of the third-nearest neighbors of a vacancy, provided a detailed insight into the effect of each jump frequency on transport coefficients for this specific alloy [16]. However, the drawback of this study lies in the complexity of the analytic expressions which depend on 16 jump frequencies, thus preventing one

*Corresponding author: thomas.schuler@cea.fr

 ©2018 American Physical Society

from gaining a general physical understanding of the most important jump frequencies. It is also possible to derive models with interactions of arbitrary range [13,38], which would require even more input parameters. These models, as well as the one by Garnier [16], allow for an accurate computation of transport coefficients but they are unsuitable for screening a large number of systems since there is no appropriate database available at present. In contrast, this paper focuses on developing an efficient screening tool to analyze simultaneously vacancy trapping by solutes and solute drag by vacancy flux in dilute fcc systems, using existing DFT data which are limited to first-nearest-neighbor interactions [39]. Note that in the five-frequency framework, models in Refs. [12,13,16,37,38] and the one developed in this paper give identical results.

In this paper, we focus on the five-frequency framework and derive simple analytic expressions for the drag ratio, which ends up being a function of two independent variables with clear physical meaning. The framework is presented in Sec. II A and analytic expressions of drag ratio are given in Sec. II B. A universal drag ratio map is built in Sec. III A, taking advantage of a diffusion database for 182 solutes in 5 distinct fcc metals [39]. Surprisingly, we find that defect trapping does not necessarily result in positive flux coupling: there are solutes with attractive binding energy to vacancies and low or even negative flux coupling (Sec. III B). In the case of positive flux coupling, we propose a kinetic model to quantify the rate of solute depletion under irradiation due to flux coupling with vacancies. This model is applied to a dilute Cu-Sb system since Sb is an effective vacancy trap which promotes interstitial-vacancy recombination (Sec. IV). Using this model, we then show that solutes are not passively dragged by defects, but they modify both defect transport coefficients and driving forces for elimination to sinks, hence altering point-defect fluxes (Sec. V).

II. DIFFUSION MODEL

A. Five-frequency framework for dilute fcc systems

The kinetic properties of the system are described within the framework of the five-frequency model [35,36] because it is simple enough to obtain analytic expressions of the drag ratio, which makes it a powerful screening tool to identify solutes with specific diffusion properties. Moreover, a recent high-throughput *ab initio* study provides the data required for this model for a total of 182 solutes, considering 5 distinct fcc matrices: Al, Cu, Ni, Pd, and Pt [39]. The five-frequency model aims at computing kinetic properties of a dilute solid solution where solute migration occurs via solute-vacancy exchanges. The system is assumed to be dilute both in vacancies V and solutes B, so that there are only two contributions to matter transport: the first contribution is that of an isolated vacancy in the bulk, and the second is that of a vacancy interacting with one solute atom. The V-B interaction, quantified by a binding energy E_b, is assumed to be restricted to first-nearest neighbors. A transition between two states being characterized by the couple {initial state; final state}, it follows that there are five different jump frequencies, shown in Fig. 1: V bulk migration (ω_0); V jump around the solute linking two configurations

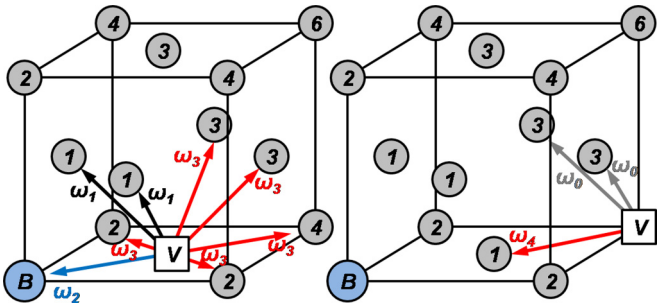

FIG. 1. Five-frequency framework for dilute fcc systems. The blue sphere, gray spheres, and white square represent a solute, matrix atoms, and a vacancy, respectively. The number on matrix atoms is the nearest-neighbor distance with respect to solute B. Arrows indicate the five different jump types considered in this model.

where V and B are first-nearest neighbors (ω_1); vacancy-solute exchange (ω_2); V jump away from the solute (ω_3); and the reverse jump to a first-nearest-neighbor site of the solute (ω_4). Note that all dissociation jumps are assumed to be equivalent, regardless whether the V jumps towards a second-, third-, or fourth-nearest-neighbor configuration. From transition-state theory [40], these jump rates are expressed using the Arrhenius law $\omega_i = \nu_i \exp(-E_m^i/k_BT)$, where ν_i is the attempt frequency and E_m^i is the migration energy, k_B is the Boltzmann constant, and T is the absolute temperature.

In the original framework of the five-frequency model, an analytic expression was given for the solute diffusivity [35,36]. This coefficient alone does not describe the full kinetic properties of the system. Indeed, following the thermodynamics of irreversible processes [25,41,42], $n(n+1)/2$ transport coefficients are required to fully describe the flux of species resulting from an arbitrary set of driving forces in an isotropic and isothermal system containing n defects or solutes. Here, the only driving forces that we need to consider are chemical potential gradient and the fluxes of V and B are expressed as

$$\begin{pmatrix} J_V \\ J_B \end{pmatrix} = -\begin{pmatrix} L_{VV} & L_{VB} \\ L_{BV} & L_{BB} \end{pmatrix} \begin{pmatrix} \frac{\nabla(\mu_V - \mu_M)}{k_BT} \\ \frac{\nabla(\mu_B - \mu_M)}{k_BT} \end{pmatrix}, \quad (1)$$

where L_{VV}, L_{BB} and $L_{VB} = L_{BV}$ are the transport coefficients and μ_M is the chemical potential of a matrix atom. Analytic expressions of these transport coefficients can be obtained, for instance, using the self-consistent mean field theory (SCMF) [11,12], as we recall below.

B. Analytic expression of the drag ratio

We use the SCMF theory to compute the drag ratio, defined as L_{VB}/L_{BB}, for dilute fcc systems. This method has already been applied to such systems [12,16] but this work establishes that, within the five-frequency framework, the drag ratio is only a function of two independent variables. In the SCMF theory, a chemical potential gradient is applied to the system which thus deviates from its equilibrium state. A thermodynamically averaged master equation enables the computation of the flux that results from this driving force and then the identification of transport coefficients as a function of atomic jump rates. The main steps are given in Appendix A and a general, detailed description of this method can be found elsewhere [12,19].

The transport coefficients obtained from the SCMF theory depend on the probability that a given jump occurs, expressed as $p_i\omega_{ij}$, where p_i is the probability of being in configuration i and ω_{ij} is the transition frequency from configuration i to configuration j. Detailed balance at equilibrium leads to $p_i\omega_{ij} = p_j\omega_{ji}$. Let E_b^i be the binding energy of configuration i, with the convention that positive values indicate attraction with respect to a configuration where solutes and point defects are infinitely separated from each other:

$$p_i\omega_{ij} = \exp\left(\frac{E_b^i}{k_BT}\right)\nu_{ij}\exp\left(-\frac{E_m^{ij}}{k_BT}\right) = \nu_{ij}\exp\left(-\frac{E_{sp}^{ij}}{k_BT}\right), \quad (2)$$

where $E_{sp}^{ij} = E_m^{ij} - E_b^i$ is the energy of the saddle-point configuration between configurations i and j. Equation (2) is general, but note that in the five-frequency framework listed above, only first nearest-neighbor binding is considered, and notations are simplified since there is only one binding energy E_b and only one subscript to specify the transitions.

Equation (2) shows that the saddle-point energy between two configurations (and not migration energies) is the quantity that matters to characterize a transition, and thus to compute transport coefficients. In the five-frequency framework, ω_3 and ω_4 are reverse jumps from each other; hence, they share the same saddle-point configuration and should not be considered as distinct variables. This is why they are both shown in red in Fig. 1. We choose the reference state for saddle-point energies as the energy of the saddle-point configuration of an isolated vacancy migrating in the pure solvent, which is mathematically equivalent to factorizing out ω_0 in each jump frequency. These ω_0 factors then cancel out when taking the ratio of two transport coefficients. Moreover, the drag ratio does not depend on the ω_2 rate because both L_{VB} and L_{BB} coefficients are proportional to ω_2 (see Appendix A). In the end, the drag ratio only depends on two reduced jump rates in the five-frequency framework: W_1 and W_3, where $W_i = p_i\omega_i/p_0\omega_0$. For convenience, we use variable $\tilde{W}_1 = W_1/W_3$ instead of W_1 to express the drag ratio

$$W_3 = \frac{\nu_3}{\nu_0}\exp\left(\frac{E_m^0 + E_b - E_m^3}{k_bT}\right), \quad (3)$$

$$\tilde{W}_1 = \frac{\nu_1}{\nu_3}\exp\left(\frac{E_m^3 - E_m^1}{k_bT}\right). \quad (4)$$

As shown in Appendix A for the system of interest here, the transport coefficients can be expressed as $L_{ij} = a^2\omega_0 Q_{ij}^\theta/Q_0^\theta$, where a is the lattice parameter, Q^θ is a θth-order polynomial function of jump rates $\{W_i\}$, where θ is the number of effective interactions that correspond to configurations from which it is possible to perform at least one jump that is not bulklike. Q_0^θ being the same for all transport coefficients, the drag ratio is simply a ratio of two θth-order polynomial functions of reduced jump rates. For vacancy-mediated diffusion in a dilute isotropic crystal, θ is the number of effective interactions located in a volume containing all atomic sites that are at most one jump away from the farthest solute-vacancy interaction distance. In the five-frequency framework for fcc crystals, the interaction distance is limited to first-nearest neighbors; one vacancy jump away from this configuration includes up to fourth-nearest-neighbor configurations. Lastly, in the out-of-equilibrium system, there are two nonsymmetrically equivalent interactions at third-nearest-neighbor distance, and therefore $\theta = 5$.

Using the notations from Eqs. (3) and (4), we used the SCMF theory to derive a compact analytic expression of the drag ratio in dilute fcc systems:

$$\frac{L_{VB}}{L_{BB}} = \frac{\tilde{W}_1P_0 + P_1}{\tilde{W}_1P_0 + P_2}, \quad (5)$$

where P_j is a fourth-order polynomial function of variable W_3,

$$P_j = \sum_{k=0}^{4}\alpha_{j,k}W_3^k, \quad (6)$$

and the $\alpha_{j,k}$ coefficients computed using the SCMF theory are provided in Table II (see Appendices A and B for details).

III. GENERAL APPROACH TO SOLUTE DRAG IN fcc ALLOYS

A. Drag ratio map

In the previous section, we have shown that in the five-frequency framework, the drag ratio depends on two variables only, and a compact analytic form has been obtained [Eq. (5)]. In Ref. [39], attempt frequencies were computed *ab initio* for 182 solutes divided among 5 fcc matrices, using the hopping-atom approximation [14,43,44]. Direct inspection of this database [39] shows that the attempt frequency ratios ν_3/ν_0 and ν_1/ν_3 vary between 0.63 and 2.00. Furthermore, a detailed study in Ref. [14] showed that the hopping-atom approximation is accurate within a factor of ∼2–3. Thus, we will consider these ratios equal to unity to simplify the discussion. This simplification does not reduce the range of applicability of our results because, at any given temperature, an attempt frequency ratio distinct from unity can be reexpressed as a shift in activation energies of the corresponding jump frequencies. If prefactors are not equal to unity, Fig. 2 remains unchanged but the energy values of each axis are shifted by some entropy value $\ln(\nu_j/\nu_i)$.

Figure 2 shows the value of the drag ratio L_{VB}/L_{BB} obtained from Eq. (5), which depends on two variables only: $(E_m^0 + E_b - E_m^3)/k_BT$ and $(E_m^3 - E_m^1)/k_BT$. Because of the normalization of energies by k_BT this map is independent of temperature. The -1.28 contour corresponds to the drag ratio obtained for a tracer matrix atom (i.e., a solute which is similar to matrix atoms such that there is no vacancy-solute binding energy) for which $L_{VB}/L_{BB} = -1/f_0$, $f_0 = 0.78146$ being the well-known fcc tracer correlation factor [24]. The fact that the drag ratio is negative when there is no solute-vacancy interaction comes from the vacancy-mediated migration mechanism, where solute and vacancy flow in opposite directions when they exchange positions. The drag ratio becomes positive when the vacancy has a higher probability to diffuse around the solute and exchange again with it rather than to diffuse away from the solute. From Fig. 2, vacancy-solute drag (positive drag ratio) occurs if at least one of two conditions is met: (1) the energy barrier for V to diffuse away from the solute is at least $\sim 2k_BT$ higher than the energy barrier to diffuse

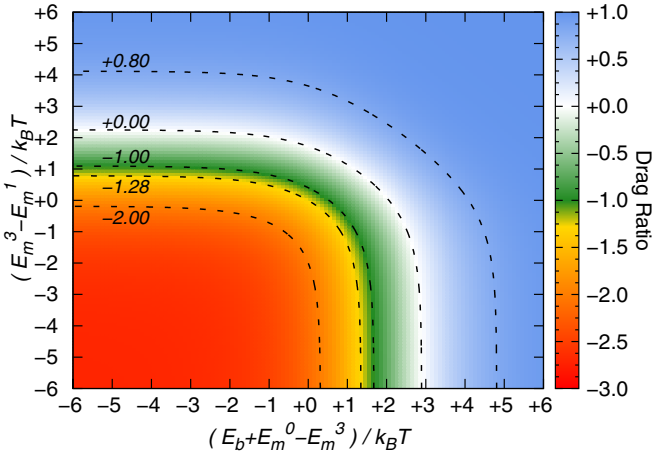

FIG. 2. Numerical evaluation of the drag ratio computed with the SCMF method in the five-frequency framework [see Eq. (5)]. Contour lines are represented for several values of the drag ratio: −2.00, −1.28, −1.00, 0.00, +0.80.

around the solute; (2) the saddle-point energy associated with a dissociation jump ($E_m^3 - E_b$) is at least $\sim 3k_BT$ lower than the saddle-point energy associated with the migration of an isolated vacancy (E_m^0). The $L_{VB} = 0$ contour does not exactly consist of two straight lines (one vertical at $3k_BT$ and one horizontal at $2k_BT$), as vacancy-solute drag can also occur when both of these conditions are nearly met simultaneously. Physically, these conditions express the fact that positive drag ratio requires a correlated motion of V around the solute. If the vacancy systematically dissociates after exchanging with the solute, vacancy-solute exchanges become random which leads to negative flux coupling (as in the tracer matrix atom example). Successive solute-vacancy exchanges are possible if the vacancy dissociation probability is low compared with the exchange probability. In the five-frequency framework, this dissociation requires basically two jumps: first V has to jump from a first-nearest-neighbor configuration to second-, third-, or fourth-nearest-neighbor configurations, and then V must not come back to a first-nearest-neighbor site, which is consistent with the above conditions for positive drag ratio: condition 1 corresponds to the fact that V has a higher probability to perform ω_1 jumps than ω_3 jumps, and condition 2 corresponds to the fact that, following a ω_3 jump, V has a higher probability to jump back to a first-nearest-neighbor configuration than to diffuse away from the solute. Note that the calculation also includes more complicated trajectories, involving dissociation, one or more bulklike jumps away from the solute, and then the same number of jumps back towards the solute and a reassociation jump. The maximum extent of these kinetic trajectories is parametrized by the correlation radius (see Appendix B).

B. Drag ratio vs fraction of trapped defects

In this section, we show that contrary to what might be expected, there exist solutes able to trap a significant fraction of vacancies while having a negative vacancy-solute flux coupling. This is surprising at first since a high binding energy is required to trap a significant fraction of vacancies, and this high binding energy is expected to create a deep energy basin from which it is hard to escape, so that the vacancy does not dissociate from the solute very often but rather migrates along with the solute, hence creating a positive flux coupling between vacancies and solutes.

First, we show that for correlating drag ratio to vacancy trapping efficiency, it is reasonable for most solutes to assume that $E_m^3 = E_m^0$, which enables to express the drag ratio as a function of variables $\tilde{W}_3 = \exp(E_b/k_BT)$ and $\tilde{W}_1$ [instead of W_3 and $\tilde{W}_1$, see Eqs. (3) and (4)]. This will be convenient because the fraction of vacancies trapped by solutes $F_T(V)$ directly depends on $\tilde{W}_3$,

$$F_T(V) = \frac{[VB]}{[V] + [VB]} = \frac{1}{1 + \dfrac{1}{12[B]\tilde{W}_3}}, \tag{7}$$

where $[V]$, $[B]$, and $[VB]$ are the concentrations of isolated vacancy, isolated solute, and vacancy-solute pair, respectively. To be consistent with the five-frequency framework, we assume that trapping only occurs when V and B are first-nearest neighbors, and there are 12 such configurations per site on the fcc lattice. The second equality in Eq. (7) stems from the assumption of local equilibrium: $[VB] = 12\exp(E_b/k_BT)[V][B]$.

In order to apply our approach to a large number of alloy systems, we took advantage of the migration energy data computed *ab initio* for 182 solutes divided among 5 different fcc matrices (Al, Cu, Ni, Pd, Pt) [39]. The first-nearest-neighbor binding energy is determined as the difference $E_m^3 - E_m^4$. This approximation holds as long as the fourth-nearest-neighbor binding is small (this configuration was used to compute dissociation barriers). Figure 3 shows the correlation between binding energies and three migration energies differences: $E_m^1 - E_m^0$ (left), $E_m^2 - E_m^0$ (center), and $E_m^3 - E_m^0$ (right). The difference $E_m^1 - E_m^0$ is, on average, roughly proportional to the binding energy, but there are significant deviations from this linear relation. The difference $E_m^2 - E_m^0$ does not seem to be correlated to the binding energy, except from a qualitative trend: solutes with higher binding energy tend to have lower exchange energy barriers. This is expected because solutes with high binding energies to vacancies usually relax toward the vacancy. As a result, they are closer to other symmetrically equivalent first-nearest-neighbor configurations, and jumping to these configurations is easier. For the third possible correlation investigated here, however, it is found that there exists a strong correlation $E_m^3 \simeq E_m^0 \pm 0.11$ eV for nearly all solutes. There are only three exceptions that fall out of this range: La and Y in Pt and S in Al. For comparison, bulk vacancy migration energies E_m^0 amount to 0.58 eV (Al), 0.72 eV (Cu), 1.09 eV (Ni), 0.96 eV (Pd), and 1.22 eV (Pt) [39].

Next, we illustrate that assuming $E_m^3 = E_m^0$ is not detrimental to the prediction of the sign of the drag ratio. To this end, Fig. 4 displays the contour obtained from Eq. (5) assuming $E_m^3 = E_m^0$ (black line). In that figure, each symbol corresponds to one solute in each matrix, and specifies the "true" sign of the drag ratio at $T = 0.5T_m$, i.e., obtained without assuming $E_m^3 = E_m^0$: an empty symbol indicates negative flux coupling and a filled symbol indicates positive flux coupling. The five different host matrices are identified by different symbol types

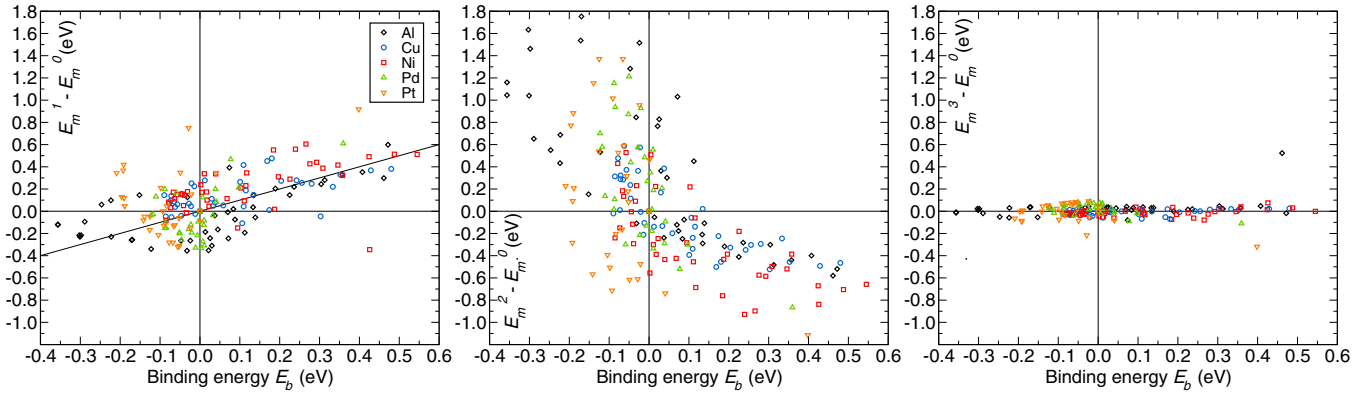

FIG. 3. Correlation between solute-vacancy binding energy and the migration barriers for vacancy jump around the solute (left), vacancy-solute exchange (center), and vacancy jump away from the solute (right). Each of the 182 points corresponds to a solute in a fcc matrix (matrices are distinguished by the color and type of symbol) and all the required data are taken from Ref. [39]. The coordinates of each point are provided as Supplemental Material [45].

and T_m is the melting temperature of the host matrix. Hence, if the above assumption leads to the correct sign of flux coupling, there should be only empty symbols below the solid curve, and only filled symbols above it. This is mostly true, except for a small number of solutes located near the boundary, where the sign of the flux coupling can be very sensitive to small changes in migration barriers. In this narrow region, however, the flux coupling is close to zero. Overall, we thus conclude that the qualitative nature of the flux coupling phenomenon is well reproduced using the simplifying assumption $E_m^3 = E_m^0$.

Finally, using the fact that $E_m^3 = E_m^0$ is a safe approximation, Fig. 5 shows the drag ratio as a function of the fraction of vacancies trapped by solutes for a solute concentration $[B] = 1$ at. %. As a baseline for trapping efficiency, we define the fraction of randomly trapped vacancies as the probability for a vacancy to be next to a solute when there is no binding energy between them and this condition is represented as a solid black line in Fig. 5:

$$F_T^0(V) = \frac{1}{1 + \dfrac{1}{12[B]}} \simeq 0.107. \tag{8}$$

The dashed contour lines are the same as in Fig. 2. For each solute in fcc matrices in Ref. [39] there is a corresponding data point on the plot (where the coordinates are evaluated at $0.5T_m$ for each matrix). The background color for drag ratio values assumes $E_m^3 \simeq E_m^0$, which predicts the correct drag ratio sign for most solutes (see Fig. 4) but not necessarily the correct magnitude. The main result in this figure is that there

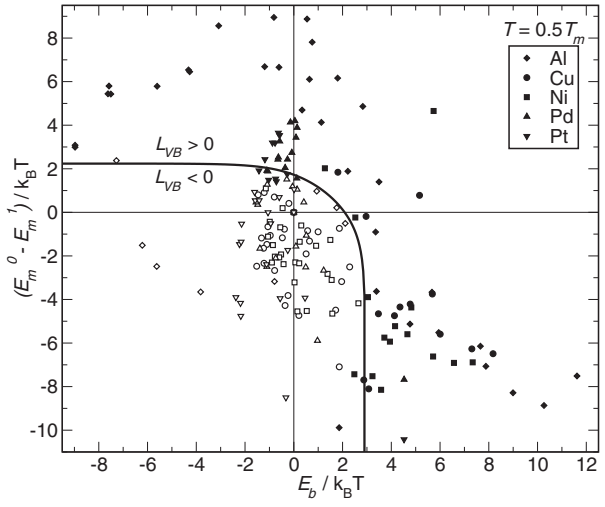

FIG. 4. The black line shows the analytic contour for $L_{VB} = 0$, assuming $E_m^3 \simeq E_m^0$. At $T = 0.5T_m$, for all 182 solutes in fcc matrices contained in Ref. [39], the sign of the drag ratio without this simplifying assumption is negative for empty symbols and positive for filled symbols. There are only a few solutes for which assuming $E_m^3 \simeq E_m^0$ would predict the wrong sign for L_{VB}. Note that the abscissa of each data point is reported assuming $E_m^3 = E_m^0$. The coordinates of each point are provided as Supplemental Material [45].

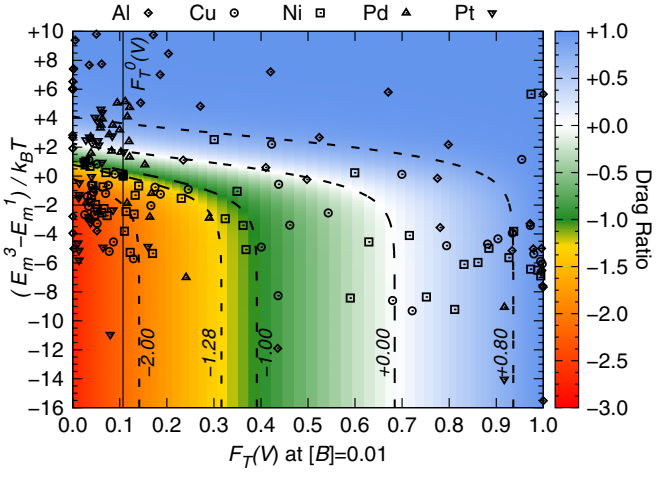

FIG. 5. The color map shows the magnitude of the drag ratio as a function of the fraction of trapped vacancies $F_T(V)$ and the migration energy difference $(E_m^3 - E_m^1)/k_BT$. The fraction of trapped vacancies is computed for a solute concentration $[B] = 1$ at. %. The solid black line corresponds to $F_T^0(V)$, the fraction of trapped vacancies when $E_b = 0$. The open symbols show the location of all 182 solutes in fcc matrices computed at $T = 0.5T_m$ with data from Ref. [39]. The coordinates of each point are provided as Supplemental Material [45].

exist solutes with significant trapping efficiency with weakly positive or even negative drag ratio. Note that the trapped fraction of vacancies is a function of temperature [Eq. (7)] and converges towards $F_T^0(V)$ as temperature increases [Eq. (8)].

IV. APPLICATION: MODEL FOR SOLUTE DEPLETION UNDER IRRADIATION

When solutes are added to a system to provide defect trapping, or solution strengthening, it is of prime importance that they remain in the solid solution but, as discussed in the previous section, flux coupling may drag these solutes towards point-defect sinks such as dislocations, grain boundaries, free surfaces, or precipitate-matrix interfaces. Figure 5 shows that there exist solutes acting as efficient vacancy traps while having a negative or small positive drag ratio. Our analysis conducted for vacancy-solute interactions suggests that it might also occur for self-interstitial defects. As one would expect, Fig. 5 also shows that most solutes that are efficient vacancy traps have a positive drag ratio. It does not mean that these solutes cannot be used for radiation enhancement or solution strengthening purposes, but that the rate at which such solute would be leaving the matrix must be taken into account when selecting a given solute, and its concentration.

In this section, we supplement the information captured in Fig. 5 by deriving a kinetic model to predict the rate of solute depletion from the matrix. We will focus here on a solute that results in a positive drag ratio and consider the situation where this alloy is subjected to irradiation because we can use well-established homogeneous rate equations to compute all needed quantities [1,2]. Regardless of the density, type, efficiency, and geometry of point-defect sinks, we assume that they can be represented altogether by an effective sink strength k^2. Point defects created by irradiation in the solid solution can either recombine or eliminate at sinks. Only the latter will lead to long-range solute redistribution and potentially solute depletion in the solid solution. The ratio of point defects that recombine to the ones created is the fraction of recombined point defects F_R, which is obtained from standard rate theory equations. Let ϕ be the irradiation flux in displacement per atom (dpa) per second and γ the fraction of the point defects produced as isolated point defects. With these definitions, the total loss of point defects to sinks per unit time is given by $\gamma\phi(1-F_R)$. The overall rate of solute depletion from the matrix is the result of two contributions, namely, the solute dragged to sinks due to flux coupling and the possible solute diffusion back to the matrix owing to the solute concentration profile built by the first contribution. In deriving the expression for the first contribution, it is assumed that there is no solute chemical potential gradient between the bulk and sinks. From Eq. (1), the flux ratio between vacancies V and solute B is

$$\frac{J_B}{J_V} = \frac{-L_{BV}\nabla\frac{\mu_V-\mu_M}{k_BT}}{-L_{VV}\nabla\frac{\mu_V-\mu_M}{k_BT}} = \frac{L_{BV}}{L_{VV}} = \frac{L_{BV}}{L_{BB}}\frac{L_{BB}}{L_{VV}}, \quad (9)$$

where the last equality isolates the contribution from the drag ratio L_{BV}/L_{BB}.

The L_{VV} coefficient can be written in the form (see Appendix A or Ref. [2])

$$L_{VV} = \frac{[V]a^2\omega_0}{\Omega} + \frac{z_{VB}[V][B]L_{VV}^{VB}}{\Omega}, \quad (10)$$

where L_{VV}^{VB} is the vacancy-solute pair contribution to the L_{VV} coefficient and the first term is the contribution from isolated vacancies. Ω is the atomic volume and $z_{VB} = 12\exp(E_b/k_BT)$ is the pair partition function, i.e., the ratio of the probability of V and B being first-nearest neighbors over the probability of V and B being isolated. Similarly, $L_{BB} = z_{VB}[V][B]L_{BB}^{VB}/\Omega$ and $L_{BV} = z_{VB}[V][B]L_{BV}^{VB}/\Omega$, such that the flux ratio becomes

$$\frac{J_B}{J_V} = \frac{\frac{L_{BV}}{L_{BB}}}{\frac{L_{VV}^{VB}}{L_{BB}^{VB}} + \frac{a^2\omega_0}{z_{VB}[B]L_{BB}^{VB}}} = \frac{1}{\eta}\frac{L_{BV}}{L_{BB}}, \quad (11)$$

where η characterizes the efficiency of the drag ratio L_{BV}/L_{BB}. Now, we write the time derivative of the total (isolated B and VB pairs) bulk solute concentration $[\bar{B}]^{\text{bulk}}$ due to vacancy drag:

$$\left.\frac{d[\bar{B}]^{\text{bulk}}}{dt}\right|_{\text{drag}} = -\frac{L_{BV}}{L_{BB}}\frac{\gamma\phi(1-F_R)}{\eta}. \quad (12)$$

As solute diffuses to point-defect sinks, the solute concentration at sinks increases, while the bulk solute concentration decreases, creating a solute concentration gradient, which is a driving force for solutes to come back to solid solution. The second step in our derivation is to quantify this second kinetic contribution. Starting from the continuity equation integrated over space and applying the divergence theorem

$$\frac{dN_B}{dt} = S_{\text{sink}}J_B^{\text{sink}\to\text{bulk}}, \quad (13)$$

where N_B is the total number of B atoms in the solid solution, S_{sink} is the total surface of point-defect sinks, and $J_B^{\text{sink}\to bulk}$ is the flux of atoms B from point-defect sinks (segregated regions) towards the bulk:

$$\begin{aligned} J_B^{\text{sink}\to bulk} &= -\frac{L_{BB}^{\text{sink}}}{a+\lambda}\frac{\mu_B^{\text{bulk}}-\mu_B^{\text{sink}}}{k_BT} \\ &= \frac{L_{BB}^{\text{sink}}}{a+\lambda}\ln\left(\frac{[B]^{\text{sink}}}{z_B^{\text{sink}}[B]^{\text{bulk}}}\right), \end{aligned} \quad (14)$$

where a is the average half-width of the segregation zone around point-defect sinks, which is typically on the order of the lattice parameter; λ is the average half-distance between two point-defect sinks; $[B]^{\text{sink}}$ and $[B]^{\text{bulk}}$ correspond to the isolated solute concentration at sinks and in the solid solution, respectively; $z_B^{\text{sink}} = \exp(E_B^{\text{sink}}/k_BT)$ with E_{Bsink} the segregation energy of solutes B at sinks. Assuming that point defects are at equilibrium around sinks, $L_{BB}^{\text{sink}} = z_{VB}[V]^{\text{eq}}[B]^{\text{sink}}L_{BB}^{VB}/\Omega$, hence,

$$J_B^{\text{sink}\to bulk} = \frac{z_{VB}[B]^{\text{sink}}[V]^{\text{eq}}L_{BB}^{VB}}{\Omega(a+\lambda)}\ln\left(\frac{[B]^{\text{sink}}}{z_B^{\text{sink}}[B]^{\text{bulk}}}\right). \quad (15)$$

To go further, we assume a planar geometry to model point-defect sinks. The bulk volume is then given by $2\lambda S_{\rm sink}$, while the volume of the segregation zone is $2aS_{\rm sink}$. The overall kinetic equation for the solute evolution is obtained by superposing Eqs. (12) and (15):

$$\frac{d[\bar{B}]^{\rm bulk}}{dt} = -\frac{a}{\lambda}\frac{d[\bar{B}]^{\rm sink}}{dt} = \frac{L_{BV}}{L_{BB}}\frac{\gamma\phi(F_R-1)}{\eta} + \frac{z_{VB}[B]^{\rm sink}[V]^{\rm eq}L_{BB}^{VB}}{2\lambda(a+\lambda)}\ln\left(\frac{[B]^{\rm sink}}{z_B^{\rm sink}[B]^{\rm bulk}}\right). \quad (16)$$

The parameters in Eq. (16) depend on different physical variables: a and λ depend on the microstructure; $[V]^{\rm eq}$, L_{BB}^{VB} and the drag ratio L_{BV}/L_{BB} depend on temperature; η depends on temperature and chemical composition; $\gamma\phi$ depends on irradiation conditions; and F_R is a function of all these variables, as detailed in Ref. [2]. Once all the values of these variables are specified, a time integration of Eq. (16) can be performed to predict the evolution of the solute concentration in the solid solution as a function of the irradiation dose.

As an example, we consider the case of solute depletion due to flux coupling in a Cu solid solution with 1 at. % Sb because all thermodynamic and kinetic parameters have been computed accurately from *ab initio* calculations for this system [2]. Sb solutes bind strongly with vacancies ($E_b = 0.38$ eV) but mixed dumbbells containing Sb are unstable in Cu. Hence, the flux coupling phenomenon under irradiation reduces to that between vacancies and Sb atoms. The corresponding drag ratio is positive at low temperature and decreases with increasing temperature, becoming negative at approximately 1200 K. Figure 6 shows the evolution of the fraction of recombined point defects F_R as a function of the dose for various temperatures and irradiation fluxes, computed for sink strengths $k^2 = 10^{14}$ m^{-2} and $k^2 = 10^{16}$ m^{-2}, corresponding to average grain diameters of 600 and 60 nm, respectively.

For the sake of simplicity, we chose $z_B^{\rm sink} = 1$ (no solute binding to sinks) and $\gamma = 1$ (irradiation producing only isolated Frenkel pairs and thus ϕ corresponding to the so-called NRT displacement rate [46,47]). However, in particular for neutron and ion irradiations, γ is lower than 1 [48–51] since some Frenkel pairs spontaneously recombine or form clusters in displacement cascades. For a given value of γ, this effect can be taken into account using the data provided in Fig. 6: in a first step, one would select the curve obtained for a displacement rate γ times smaller than the NRT one, and in a second step, the dose of interest, for instance the inflection point on the curve, would be increased by γ, yielding the corresponding NRT dose.

In this work, the value of η was obtained from atomic-scale jump frequencies using the expressions provided in Appendix A. Note that when the vacancy solute pair is strongly bound ($E_b \gg 3k_BT$), an approximate but accurate value of η can be obtained from experimental data that are available for most binary alloys (self-diffusion $D^*_{\rm self}$ and solute D^*_B tracer diffusion coefficients) [2]: $\eta \simeq 1 + D^*_{\rm self}/[B]f_0D^*_B$.

As the system evolves, solutes are lost to sinks due to flux coupling with vacancies, hence the decrease in the fraction of recombined point defects. This decrease depends both on temperature and irradiation flux. For a given irradiation flux, lower temperatures lead to larger decrease in the fraction of recombined point defect at steady state, the evolution of F_R with dose is sharper, and starts at a lower dose. At a given temperature, as the irradiation flux increases, the difference between initial and steady state F_R is larger and solute depletion starts at higher doses. At temperatures higher than 550 K, the loss of solutes over time becomes smaller because flux coupling and vacancy trapping decrease. Moreover, for each temperature, the fraction of recombined point defects is sensitive to the solid solution solute content over a limited irradiation flux domain only [2]. Outside of this domain, the loss of solutes to sink does not affect much F_R. Comparing the two graphs in Fig. 6, one can see that higher sink strength shifts this irradiation flux domain to higher displacement rates for a given temperature, but the qualitative features of the F_R decrease with dose remain the same.

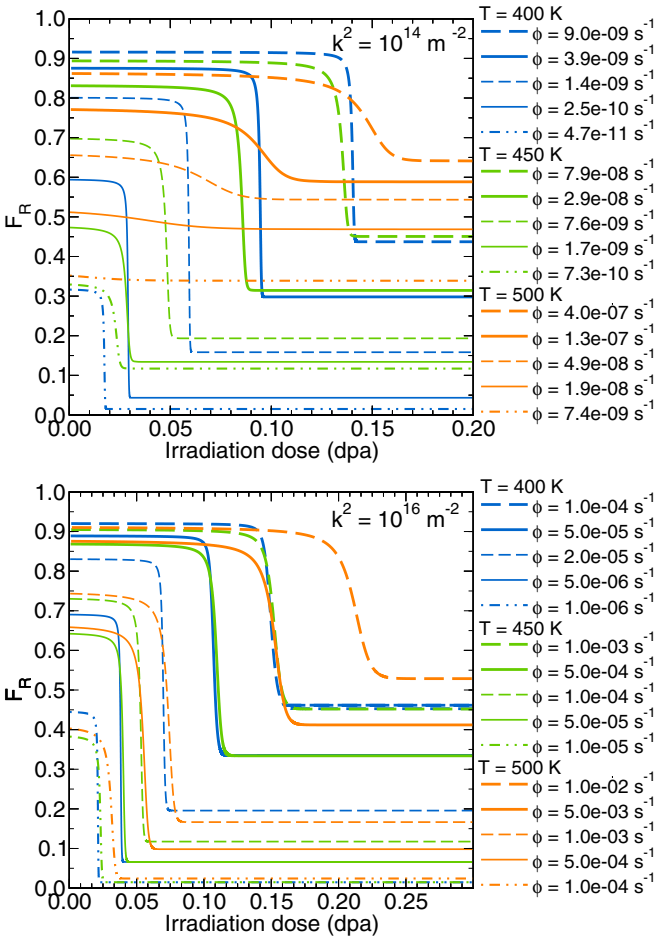

FIG. 6. Evolution of the fraction of recombined point defects (which depends on solute concentration) as a function of the irradiation dose computed for $\gamma = 1$. Displacement rates are given in dpa/s.

V. DISCUSSION

We considered here the case of solutes that are used to enhance the relative rate of recombination under irradiation, so as to reduce the potentially detrimental effects brought about

by long-range diffusion of point defects and chemical species. Since no solute can be a perfect trap at finite temperature, it is important to determine whether fluxes of point defects, and specifically vacancies, to sinks will result in a progressive removal of the solute from the matrix and segregation at the sinks. A first important result from our systematic investigation of 182 solutes in 5 distinct fcc matrices is that there exist trapping solutes with negative flux coupling with vacancies. As seen in Fig. 5, it is easier for vacancies to dissociate from these solutes than to migrate around them, while the corresponding vacancy-solute binding energy is such that $12[B]\hat{W}_3 \simeq 1$, meaning that about half of the vacancies in the system are trapped.

Since many vacancy-trapping solutes display a positive flux coupling with vacancies, it is important to estimate how fast this flux coupling would remove solute from the matrix. We addressed this question by building a kinetic model for solute diffusion to and away from sinks under continuous irradiation. At the onset of irradiation, all the solutes are assumed to be in solution in the matrix, thus most of the vacancies are trapped, and only a small fraction of point defects diffuse to the sinks. As a consequence, at low doses, the solute flux to sinks is small, and the solute concentration in the solid solution decreases slowly. However, this removal rate increases with time because as solutes are removed from the solid solution, point-defect recombination is less efficient, thus the flux of vacancies to sinks becomes larger and larger, and consequently the coupled flux of solutes increases over time. At some dose, the curve representing the matrix solute concentration displays an inflection point (see Fig. 6) which stems from the reverse flux due to solute concentration inhomogeneities between bulk and sinks. Indeed, the segregation of solutes at sinks creates a solute concentration gradient between the sinks and the bulk, and hence a back-diffusion flux of solutes. This solute flux increases over time, thus, the bulk solute depletion rate decreases over time, until it reaches some steady-state value, where the flux of solutes to the sinks due to coupling with vacancies is balanced by the solute back-diffusion flux due to solute concentration gradient between bulk and sink. Note that the lower the initial F_R (at $\theta = 0$ dpa), the shorter the "incubation" period where solute concentration decreases slowly.

The behavior observed in Fig. 6 is in qualitative agreement with experimental features observed in Ref. [3], where the addition of oversized solutes (Hf, Zr) in austenitic steels is shown to suppress Cr radiation-induced segregation under proton irradiation, but up to a certain dose only: 3 dpa at $T = 673$ K and 1 dpa at $T = 773$ K. Their observations were analyzed with a rate-theory model [52] which is in essence similar to the one we used here except that oversized solutes were considered as immobile traps for vacancies. As a consequence, these authors could not reproduce the experimental observation of solute efficiency fading, unless assuming that the oversized solute concentration in the solid solution was decreasing with time, which was experimentally confirmed by atom-probe tomography measurements [3]. In contrast, our model captures the full kinetic interplay between solutes and vacancies, through temperature-dependent flux coupling parameters obtained from atomic-scale calculations, thus eliminating the need for any arbitrary assumption on

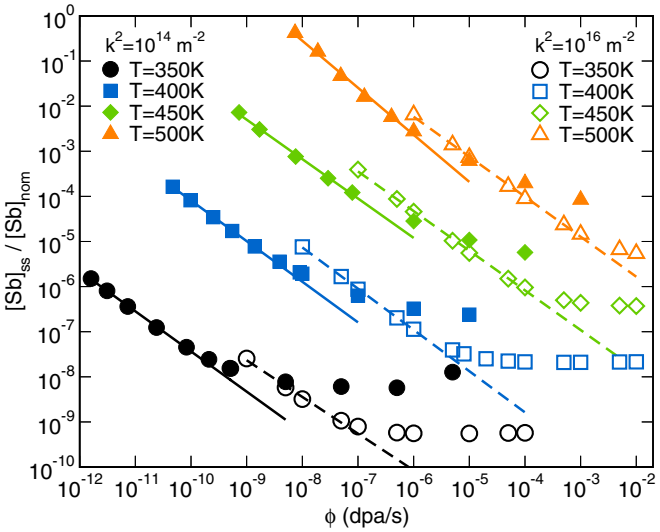

FIG. 7. Power-law relation between $[Sb]_{ss}$, the steady-state bulk concentration of Sb atoms, and the irradiation flux at various temperatures and sink strengths k^2. The power-law fit (solid and dashed lines) is only valid at low irradiation fluxes, and exponents range between -0.91 and -0.81, except for the $T = 500$ K and $k^2 = 10^{14}$ m^{-2} curve where the exponent is -1.04. At higher fluxes, the steady-state Sb concentration shows a flat minimum (see text).

the evolution of the solute concentration in the matrix. As a result, the present model computes directly the effect of solutes on point-defect recombination and thus on radiation-induced segregation and void swelling. Data provided as Supplemental Material show that Zr in Ni has binding and flux coupling coefficients that are close to that of Sb in Cu [45]. Hence, even though our calculations dealt with a model Cu-1 at. % Sb alloy, it is encouraging that they share the same features identified in Ref. [3]: there is a dose, the inflection point in Fig. 6, where solute concentration decreases sharply, such that beyond this dose, there are not enough solutes left in the solid solution to slow down vacancies, and the recombination of point defects decreases. In our model, these solutes disappear from solid solution because they segregate to point-defect sinks. In Ref. [3], it was proposed that these sinks could be matrix-carbide interfaces. In qualitative agreement with experimental observation [3], we find that for a given irradiation flux, the inflection point appears at lower dose when temperature increases.

While sink strength is taken constant in our calculations, it typically increases with time as point defect form larger, nearly immobile clusters [53]. On the one hand this effect should shift the inflection point towards lower dose values (see Fig. 8). On the other hand, however, the trapping of vacancies by solutes is likely to increase the incubation dose for point-defect cluster precipitation. This question would thus require to model simultaneously the evolution of defect clusters and solute under irradiation. This is left for future study. Finally, in the Cu-Sb calculations we did not take into account the binding energy between solutes and sinks, which would reduce the solute back-diffusion term [Eq. (15)] and thus shift the inflection point towards higher dose values.

TABLE I. Power-law parameters for the fits in Figs. 7 and 8.

	$[Sb]_{ss} = \alpha\phi^{\beta}$		$\theta_{inf} = \alpha\phi^{\beta}$	
	α	β	α	β
T (K)	$k^2 = 10^{14}$ m^{-2}			
350	4.60×10^{-15}	−0.890	6.50×10^{3}	0.495
400	8.01×10^{-12}	−0.901	1.24×10^{3}	0.490
450	6.86×10^{-9}	−0.874	3.73×10^{2}	0.482
500	1.28×10^{-7}	−1.043	1.82×10^{2}	0.487
T (K)	$k^2 = 10^{16}$ m^{-2}			
350	1.12×10^{-13}	−0.813	8.06×10^{1}	0.507
400	3.59×10^{-11}	−0.914	1.54×10^{1}	0.498
450	2.51×10^{-8}	−0.879	4.01×10^{0}	0.469
500	2.79×10^{-6}	−0.887	1.67×10^{0}	0.451

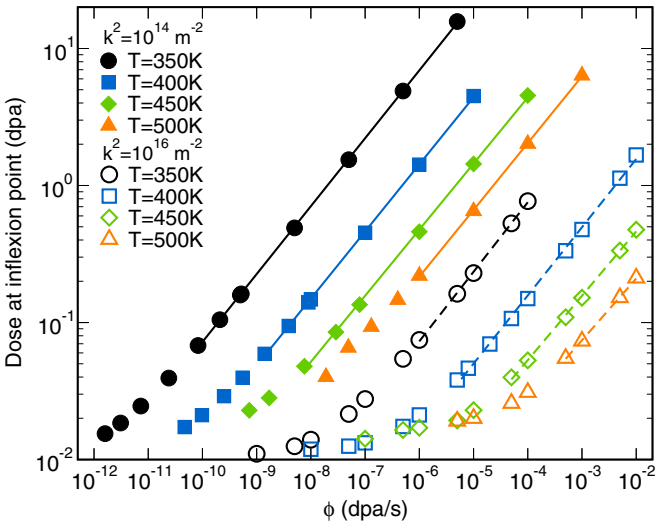

FIG. 8. Evolution of the dose at the inflection point of the curves in Fig. 6 as a function of the dose rate ϕ for various temperatures and sink strengths. At high enough irradiation flux, a power-law relation can be fitted to these results (solid and dashed lines), with exponents ranging from 0.45 to 0.51 depending on temperature and sink strength.

It is interesting to consider further the effect of temperature and irradiation dose rate on two parameters: the dose at the inflection point and the steady-state solute concentration. Starting with the latter, Fig. 7 shows that for each temperature there exists a power law between the steady-state solute concentration (with respect to the nominal solute concentration) and the irradiation flux. The coefficients of the power law depend on temperature and on sink strength, but the exponent is similar for each of them (between −0.91 and −0.81 except one of them which is −1.04, see Table I). Note that the data points used to fit this relationship all belong to the temperature/irradiation flux region where Sb atoms increase the fraction of recombined point defects by at least 20%. Indeed, when ϕ increases further, we observe a deviation from this power law and the steady-state solute concentration in the solid solution appears to saturate. Upon closer inspection of this region, the curves display in fact a flat minimum and the value of $[Sb]_{ss}$ is not rigorously independent from ϕ in this region. For the $T = 350$ K curve at $k^2 = 10^{14}$ m^{-2}, this behavior is easier to observe. At low fluxes, F_R depends on the solute concentration, which decreases over time because of flux coupling such that the steady-state F_R values are not so high and lead to substantial solute segregation. When ϕ increases, this effect is amplified simply by the fact that the flux of vacancies to sinks is higher. Admittedly, F_R also increases with ϕ but it is not enough to counterbalance the larger flux of defects, hence, the decrease of the steady-state bulk concentration with increasing ϕ. Nevertheless, at higher irradiation dose rate, F_R does not depend so much on solute concentration and remains almost constant over time, such that the steady-state F_R values get closer to 1 and the flux of point defects to sinks stays small at steady state. Hence, solute segregation is less important and the steady-state bulk concentration increases again with ϕ.

We return now to the inflection points in the solute depletion curves (see Fig. 6). Because the decrease of solute concentration in the solid solution is rather sharp in most cases, the dose at which this inflection occurs θ_{inf} is representative of the period over which the solute is efficient in maintaining a high recombination rate of point defects. Figure 8 shows the evolution of θ_{inf} as a function of dose rate, temperature, and sink strength. In the regime of large flux ϕ, the data can be fit by a power law and the exponents display little dependence with temperature and sink strength, ranging from 0.45 to 0.51 (see Table I). Note that in Fig. 7, the power-law fit is obtained in the low-ϕ region, while in Fig. 8 the fit is obtained in the high-ϕ region. At this point, there are no simple physical arguments to rationalize these power-law fits, as they result from the complex interplay between solid solution kinetic properties and irradiation parameters. Still, it is interesting to note that at "high" irradiation flux (depending on temperature and sink strength), the dose at which the solute concentration in the solid solution does not affect the fraction of recombined point defects at steady state roughly evolves as $\sqrt{\phi}$.

Finally, we would like to emphasize that Sb in Cu, and solute additions in general, have various effects on point defects that will all ultimately affect the solute depletion under irradiation. In Ref. [2] we have shown that the recombined fraction of point defects is affected by solute additions because of two phenomena: solutes slow down point defects, but also stabilize them in the solid solution. Following Onsager relations, the flux of solutes to sinks is the product of transport coefficients and chemical potential gradients [Eq. (1)]. The transport coefficients that control the flux of vacancies are expressed as the sum of the transport coefficients of isolated vacancies and vacancies paired with a solute, weighted by the probability of these configurations [Eq. (10)]. Hence, the more attractive the interaction between solute and vacancy, the more pairs in the system. If the solute slows down the vacancy, then the overall vacancy population has lower transport coefficients, meaning it diffuses more slowly. If the solute does not slow vacancies significantly, the vacancy transport coefficients increase because solute stabilizes vacancies in the solid solution: as there are more vacancies in the system, the flux of vacancies in response to a given driving force is larger. These two aspects are shown in the left-hand plot of Fig. 9 in the case of CuSb. The total L_{VV} coefficient is plotted, normalized by the one obtained in pure Cu (where all vacancies

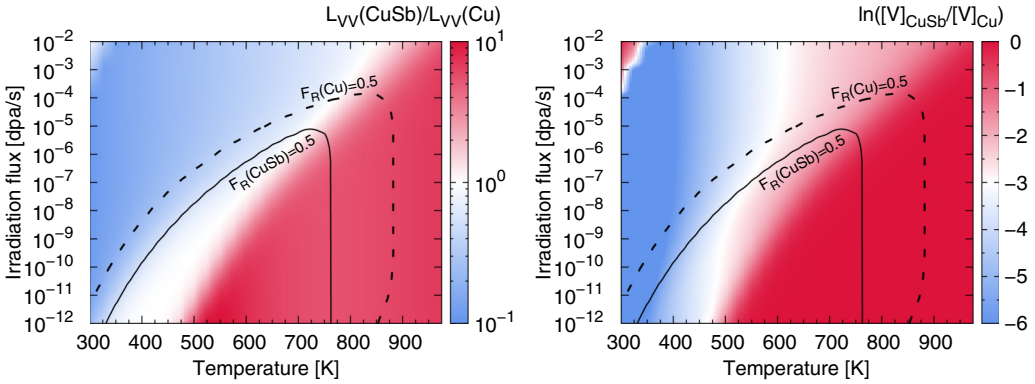

FIG. 9. Left: ratio between the total L_{VV} transport coefficient [Eq. (10)] in CuSb and in pure Cu, as a function of temperature and irradiation rate. Right: vacancy chemical potential difference in CuSb and pure Cu solid solutions, normalized by k_BT, as a function of temperature and irradiation flux. These two plots show that solutes affect both point-defect transport coefficients and driving forces for elimination at sinks.

are isolated). At low temperature/high irradiation flux, Sb atoms decrease the L_{VV} coefficient because they slow down vacancies effectively and cannot stabilize enough vacancies to counterbalance this. At higher temperature, vacancies diffuse at similar rates whether they are isolated or paired with solutes, so their concentration is higher than in pure Cu since the solutes stabilize them effectively. At first, one may think that the driving force for point-defect elimination at sinks would be higher in Cu-Sb. This is, however, not correct since the driving force for elimination is not a total point-defect concentration gradient but rather a point-defect chemical potential gradient which, under local equilibrium conditions (needed to define properly a chemical potential) is proportional to the isolated point-defect concentration gradient. The vacancy chemical potential difference normalized by k_BT between Cu-Sb solid solutions and Cu is plotted on the right-hand plot of Fig. 9. It shows that whatever the temperature and irradiation flux conditions, the driving force for vacancy elimination at sinks is actually decreased by solute additions. We can also demonstrate this analytically starting from the expressions in Ref. [2], and assuming for simplicity that the concentration of solute monomer is not affected by irradiation (which is true as long as the solute concentration is much higher than the point-defect concentration):

$$F_R = 1 - \frac{k^2 a^2 \omega_0}{\phi}\left([V] - [V]^{\mathrm{eq}}\right)(1+\Gamma), \tag{17}$$

with $\Gamma = [B] z_{VB} L_{VV}^{VB}/a^2\omega_0$. Since solute additions can only increase F_R when solutes slow down point defects, $F_R(\mathrm{CuSb}) \geqslant F_R(\mathrm{Cu})$, and thus

$$[V]_{\mathrm{CuSb}} \leqslant [V]_{\mathrm{Cu}}\left(\frac{1+\Gamma[V]^{\mathrm{eq}}/[V]_{\mathrm{Cu}}}{1+\Gamma}\right) \leqslant [V]_{\mathrm{Cu}} \tag{18}$$

because $\Gamma \geqslant 0$ and $[V]^{\mathrm{eq}} \leqslant [V]_{\mathrm{Cu}}$. As long as a solute slows down point defects, it will necessarily decrease the driving force for point-defect elimination at sinks, even if it stabilizes point defects in solid solution, thus increasing the total point-defect concentration in the system. This situation resembles what happens under equilibrium conditions: vacancy chemical potential is fixed by equilibrium conditions but the total vacancy concentration may increase upon solute additions [54]. In the end, the flux coupling phenomenon is not a function of the drag ratio only because solute additions will modify the point-defect elimination flux at sinks by altering both transport coefficients and driving forces.

VI. CONCLUSION

We have shown that in the five-frequency framework for fcc systems, the vacancy-solute drag ratio actually depends on two variables only. We provided compact expressions for the full Onsager matrix in dilute binary fcc system with vacancy-mediated diffusion, in the form of ratio of polynomial functions of jump frequency ratios. Increasing the correlation radius (volume of space where kinetic trajectories are accounted for) does not change this analytic form but leads to converged polynomial coefficients.

Using an available *ab initio* database for solute diffusion in five fcc matrices (Al, Cu, Ni, Pd, and Pt) [39], the bulk migration barrier and the dissociation barrier are found almost equal for most solutes. This is an interesting approximation since it allows to express the drag ratio as a function of two parameters: vacancy jump frequency ratio around the solute and far from the solute, and solute vacancy-binding energy. The latter is conveniently recast in the form of a fraction of trapped point defects, allowing for a systematic study of solute drag and vacancy trapping in a large number of alloys. As expected, most solutes that trap vacancies have a positive drag ratio, but an important result here is that there are some solutes that are able to trap more than half of the vacancies while having low or negative flux coupling.

For solute with positive flux coupling, we derived a simple model to compute the solute matrix depletion over time. This model converts the drag ratio information computed from the atomic scale into the time interval over which solute depletion reaches a certain level below which the remaining solute concentration in solution might no longer provide sufficient trapping of point defects. The model could be used for alloy design to determine appropriate solute concentrations and ensure materials' performances over a given time period. As an example, we applied our model to a Cu-Sb solid solution under irradiation.

For a given temperature and sink strength, the steady-state solute concentration in the solid solution evolves as $\phi^{-\beta}$ with

the exponent slightly lower than 1 in most cases. This relation is valid for low irradiation fluxes. At higher irradiation fluxes, the steady-state solute concentration is roughly constant, while the dose at which most of the solute depletion occurs evolves as $\sqrt{\phi}$. Further investigation is required to understand better these trends and generalize them to other systems.

Finally, we have shown that solutes are not simply dragged to sinks by point defects, they also directly affect the flux of point defects to sinks by modifying both transport coefficients and driving forces for elimination, i.e., point-defect chemical potential. Generally, when solutes have an attractive interaction with vacancies and slow down vacancies, they will increase the total vacancy concentration in the system and at the same time decrease the driving force for vacancy elimination.

ACKNOWLEDGMENTS

This research is supported by the U. S. Department of Energy (DOE), Office of Science, Basic Energy Sciences (BES) under Award No. DE-FG02-05ER46217.

APPENDIX A: ANALYTIC EXPRESSIONS OF THE FULL ONSAGER MATRIX FOR MATERIALS DESCRIBED IN THE FIVE-FREQUENCY FRAMEWORK

In this appendix, we derive Eq. (5) from the self-consistent mean field theory (SCMF). This equation is interesting because the drag ratio is expressed as a two-variable function, this function being a simple ratio of polynomial functions. Whereas the application of the SCMF to a dilute fcc alloy is not new, this convenient form of the drag ratio was not identified previously. Therefore, we find it useful to outline the steps leading to this expression, while the SCMF method is described in details for instance in Refs. [12,19].

The starting point of the SCMF theory is a microscopic master equation of out-of-equilibrium configuration probabilities:

$$\frac{dp_n}{dt} = \sum_m p_m \omega_{mn} - p_n \omega_{nm}, \tag{A1}$$

where p_n is the out-of-equilibrium probability of configuration n and ω_{mn} is the jump rate from configuration m to configuration n. Our goal is to compute transport coefficients in the framework of the thermodynamics of irreversible processes [Eq. (1)], therefore, we need to express a flux of species as a function of driving forces.

The flux per site is obtained from the time derivative of the first moment of the probability distribution p, using a continuity equation

$$\sum_n n_i^\alpha \frac{dp_n}{dt} = \frac{d\langle n_i^\alpha \rangle}{dt} = \sum_s j_{i\to s}^\alpha, \tag{A2}$$

where n_i^α is a site occupation number (=1 if species α is on site i and =0 otherwise) and $\langle \ldots \rangle$ represents a thermodynamic average over the out-of-equilibrium probability distribution p.

Probability distribution p is *a priori* unknown, and we assume it can be expressed as $p_n = p_n^0 \delta p_n$, where p^0 is the (known) equilibrium probability distribution, and δp is the out-of-equilibrium contribution. Both components are assumed to have the same mathematical form $p_n^0 = \exp(-\mathcal{F}_n/k_BT)$ and $\delta p_n = \exp(-\delta\mathcal{F}_n/k_BT)$, where $\mathcal{F}_n$ and $\delta\mathcal{F}_n$ are free energies. Moreover, we assume a small deviation from equilibrium ($\delta\mathcal{F}_n \ll k_BT$) such that $\delta p_n \simeq 1 - \delta\mathcal{F}_n/k_BT$. From detailed balance at equilibrium, the equation can be simplified further into

$$\sum_s j_{i\to s}^\alpha = \sum_m \left\langle n_i^\alpha \omega_{mn} \frac{\delta\mathcal{F}_m - \delta\mathcal{F}_n}{k_BT} \right\rangle^0, \tag{A3}$$

where $\langle \ldots \rangle^0$ denotes the thermodynamic average over the equilibrium probability distribution p^0. Because vacancy jumps only occur with first-nearest neighbors, the sum over sites s and the sum over configurations m are equivalent. The quantities $\delta\mathcal{F}_n$ are obtained for each symmetrically unique configuration (in the out-of-equilibrium system) from the stationarity of the second moment of probability distribution p^0 because in the homogeneous dilute system, the configuration is fully characterized by the vector between vacancy and solute: $\langle n_i^\alpha n_j^\beta \rangle = 0$. As a consequence, $\delta\mathcal{F}_n$ is found proportional to the driving forces, chemical potential gradients, which allows us to identify transport coefficients.

Without going into the details, the Onsager matrix $\mathbf{L}$ can be expressed in a matrix format where each matrix element is a linear combination of quantities $p_i\omega_i = \exp(-E_{sp}^i/k_BT)$

TABLE II. Coefficients of polynomial functions (6) obtained for a correlation radius $R_{\rm cor} = 4a$. These coefficients are obtained from SCMF calculations.

$\alpha_{j,k}$	$k=0$	$k=1$	$k=2$	$k=3$	$k=4$
$j=0$	+1.0000	+1.3508	+0.56862	+0.089534	+0.0044380
$j=1$	−9.4832	−6.3630	−1.0109	−0.0030132	+0.0044380
$j=2$	+3.5000	+3.2364	+0.96152	+0.11299	+0.0044380
$j=3$	+1631.3	+700.83	+112.12	+5.6706	+0.0044380
$j=4$	+1174.0	+1653.8	+716.79	+115.10	+5.7896
$j=5$	+4109.1	+3868.4	+1178.4	+142.66	+5.7896

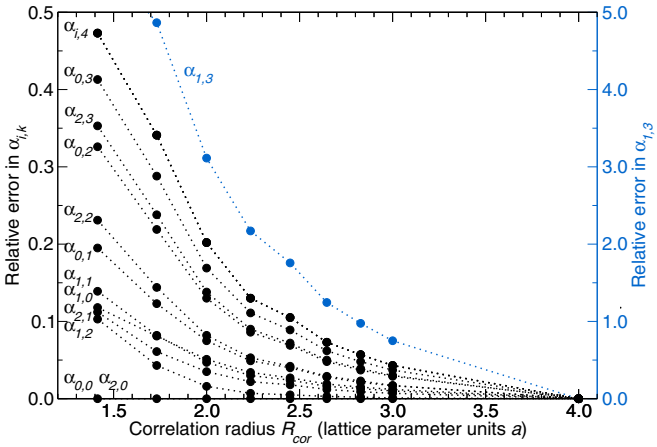

FIG. 10. Convergence of polynomial coefficients $\alpha_{i,k}$ as a function of the correlation radius. The relative error is computed with respect to the value of $\alpha_{i,k}$ computed at $R_{\rm cor} = 4a$, and absolute values are shown. Note that $\alpha_{1,3}$ is more difficult to converge than the other coefficients, hence, it is plotted on a different scale (right-hand-side axis).

for $i = 0$, 1, 2, or 3. Because of this linearity, each jump frequency can be factorized by ω_0, making the following matrices dependent of reduced jump frequencies W_i only:

$$\mathbf{L} = a^2\omega_0\left(\mathbf{L^0} - 2\mathbf{\Lambda}^t\mathbf{T}^{-1}\mathbf{\Lambda}\right), \tag{A4}$$

where $\mathbf{L}^0$ is the uncorrelated contribution while the second term in the parentheses is the correlated part of the jumps, represented by matrices $\mathbf{\Lambda}$ ($n_\sigma \times 2$ matrix) and $\mathbf{T}$ (symmetric $n_\sigma \times n_\sigma$ matrix), where n_σ is the number of symmetry-unique configurations in the out-of-equilibrium system and such that the vacancy-solute distance is lower than the correlation distance R_{cor}. As an example, these matrices are given below for $R_{\text{cor}} = 2a$, and $\mathbf{T} = \mathbf{I}_{n_\sigma}\mathbf{D} + \mathbf{C} + \mathbf{C}^t$ ($\mathbf{I}_{n_\sigma}$ being the identity matrix):

$$\mathbf{L}^0 = \begin{pmatrix} W_2 + 4W_1 + 14W_3 + 121 & -W_2 \\ -W_2 & W_2 \end{pmatrix}, \tag{A5}$$

$$\mathbf{\Lambda} = \begin{pmatrix} 3W_3 - 2W_1 - W_2 & W_2 \\ 1 - W_3 & 0 \\ W_3 - 1 & 0 \\ 2(1 - W_3) & 0 \\ 2(W_3 - 1) & 0 \\ 0 & 0 \\ | & | \\ 0 & 0 \end{pmatrix}, \tag{A6}$$

$$\mathbf{D} = \begin{pmatrix} 2W_1 + 2W_2 + 7W_3 \\ W_3 + 11 \\ W_3 + 2 \\ 2W_3 + 10 \\ 4W_3 + 18 \\ 12 \\ 10 \\ 22 \\ 24 \\ 22 \\ 12 \\ 3 \end{pmatrix}, \tag{A7}$$

$$\mathbf{C} = \begin{pmatrix} 0 & -W_3 & W_3 & -2W_3 & 2W_3 & 0 & 0 & 0 & 0 & 0 & 0 & 0 \\ 0 & 0 & 0 & -2 & 2 & -1 & 1 & -2 & 2 & 0 & 0 & 0 \\ 0 & 0 & 0 & 1 & 0 & 0 & -1 & 0 & 0 & 0 & 0 & 0 \\ 0 & 0 & 0 & 0 & 2 & 0 & 2 & -2 & 0 & 0 & -1 & 0 \\ 0 & 0 & 0 & 0 & 0 & 2 & 0 & 0 & -2 & -2 & 2 & 0 \\ 0 & 0 & 0 & 0 & 0 & 0 & 0 & 0 & 2 & 0 & 0 & 0 \\ 0 & 0 & 0 & 0 & 0 & 0 & 0 & 2 & 0 & 0 & 0 & -1 \\ 0 & 0 & 0 & 0 & 0 & 0 & 0 & 0 & 2 & 0 & -2 & 0 \\ 0 & 0 & 0 & 0 & 0 & 0 & 0 & 0 & 0 & -2 & 2 & 0 \\ 0 & 0 & 0 & 0 & 0 & 0 & 0 & 0 & 0 & 0 & 2 & 0 \\ 0 & 0 & 0 & 0 & 0 & 0 & 0 & 0 & 0 & 0 & 0 & 0 \\ 0 & 0 & 0 & 0 & 0 & 0 & 0 & 0 & 0 & 0 & 0 & 0 \end{pmatrix}. \tag{A8}$$

When actually inverting matrix $\mathbf{T}$, we provide analytic formulas for transport coefficients in the five-frequency framework, written concisely using fourth-order polynomial functions of W_3 [see Eq. (6)], whose coefficients are provided in Table II. We define $L^V_{VV} = a^2\omega_0[V]/\Omega$, the transport coefficient (in $\text{m}^{-1}\,\text{s}^{-1}$) of an isolated vacancy in a bulk system. Let us remind that W_i is a function of the saddle-point energy of jump i, not a function of migration energies. With these notations, we provide the aforementioned expressions for $R_{\text{cor}} = 4a$:

$$L_{VB} = L_{BV} = \kappa L^V_{VV} W_2(W_1P_0 + W_3P_1), \tag{A9}$$

$$L_{BB} = \kappa L^V_{VV} W_2(W_1P_0 + W_3P_2), \tag{A10}$$

$$L_{VV} = L^V_{VV}[1 + \kappa(W_2(1174 + W_1P_0 + W_3P_3) + W_1P_4 + W_3P_5)], \tag{A11}$$

$$\kappa = \frac{1024[B]}{(W_1 + W_2)P_0 + W_3P_2}. \tag{A12}$$

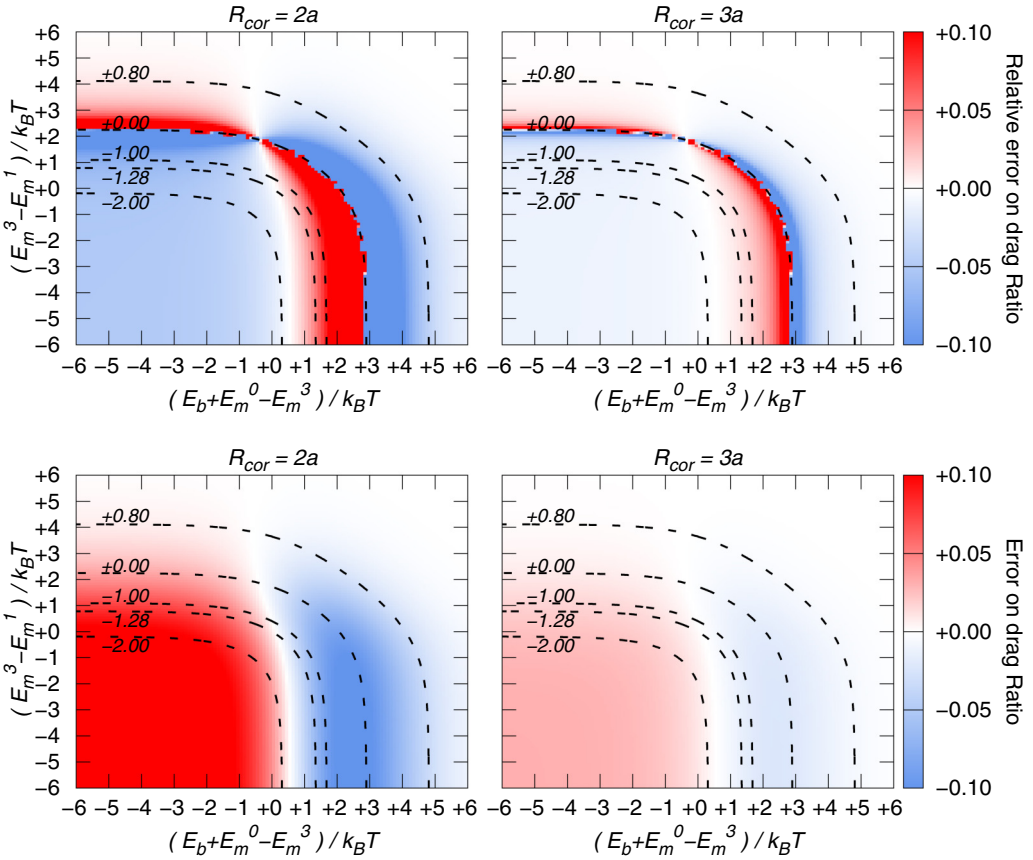

FIG. 11. Convergence of the drag ratio with respect to $R_{\rm cor}$. The top plots show the relative error on drag ratio with respect to calculations done at $R_{\rm cor} = 4a$. It is seen from the right-hand-side plot that most drag ratios are converged within less than a few percent at $R_{\rm cor} = 3a$. For drag ratios that are close to zero, the relative error seems higher (because it is divided by a small quantity), hence the bright colors corresponding to maximum relative error near the zero contour. The bottom plots show the absolute error on the drag ratio, showing that systems with low or negative $(E_m^3 - E_m^1)/k_BT$ are usually harder to converge. At $R_{\rm cor} = 3a$, the drag ratio is already converged to at least one decimal for any system.

Looking at Eqs. (A9) and (A10), we find that the drag ratio is independent of the vacancy-solute exchange frequency ω_2 [Eq. (5)].

APPENDIX B: CONVERGENCE OF TRANSPORT COEFFICIENTS WITH $R_{\rm cor}$

When increasing the correlation radius, which parametrizes the extent of the volume where kinetic trajectories are taken into account, the mathematical form of Eqs. (A9) to (A12) does not change, only the numerical coefficients of the polynomial functions are affected. In Eq. (A5), only coefficient "121" is changed to a higher value. Some lines are added to matrix $\mathbf{\Lambda}$ but the coefficients are all zeros. However, the coefficients in the lines (and columns) added to $\mathbf{D}$ and $\mathbf{C}$ are integer numerical values. As $R_{\rm cor}$ increases, so does the size of matrix $\mathbf{T}$ and the required computational effort to solve the problem, but it leads to more precise values of polynomial coefficients $\alpha_{j,k}$. Trajectories involving configurations where V and B are farther apart have a lower thermodynamic weight, such that $\alpha_{j,k}$ coefficients, and more generally speaking transport coefficients, converge with respect to $R_{\rm cor}$. The $\alpha_{j,k}$ values used in this work are given in Table II, and the convergence behavior is shown in Fig. 10. The relative error that is plotted in Fig. 10 is defined as $|1 - \alpha_{j,k}(R_{\rm cor})/\alpha_{j,k}(4a)|$. These relative errors decay according to an exponential law $\gamma_{j,k}\exp(-\lambda_{j,k}R_{\rm cor})$ with $0.97 < \gamma_{j,k} < 5.36$ and $1.34 < \lambda_{j,k} < 1.74$. There are two exceptions: $\gamma_{1,3} = 43.4$ and $\lambda_{1,2} = 2.85$. It is interesting to note that all these coefficients follow a similar law of decay, even though the physical or mathematical origin of this observation is not yet understood.

From Fig. 11, we see that the convergence of the drag ratio, which is the quantity of interest in this study, is faster than the convergence of individual $\alpha_{j,k}$ polynomial coefficients, and confirms that the physical quantities that are discussed in this paper are well converged with respect to $R_{\rm cor}$. Indeed, Fig. 11 shows the relative error in the drag ratio map of Fig. 2 when $R_{\rm cor}$ is set to $2a$ or $3a$ (with respect to the calculation done at $R_{\rm cor} = 4a$). The same contours as in Fig. 2 are shown. It is interesting to note that for $(E_m^0 + E_b - E_m^3) \gtrsim 0$ positive drag ratios are underestimated by lower $R_{\rm cor}$ values and negative drag ratio or overestimated. The opposite applies for $(E_m^0 + E_b - E_m^3) \lesssim 0$. This demonstrates that even for a simple description of the system such as the one adopted here, the convergence of the drag ratio, and more generally of transport coefficients, is not straightforward to anticipate from jump rates.

[1] L. Mansur and M. Yoo, J. Nucl. Mater. **74**, 228 (1978).
[2] T. Schuler, D. R. Trinkle, P. Bellon, and R. S. Averback, Phys. Rev. B **95**, 174102 (2017).
[3] M. J. Hackett, J. T. Busby, M. K. Miller, and G. S. Was, J. Nucl. Mater. **389**, 265 (2009).
[4] T. R. Anthony, Phys. Rev. B **2**, 264 (1970).
[5] M. Nastar and F. Soisson, Comprehensive Nucl. Mater. **1**, 471 (2012).
[6] A. J. Ardell and P. Bellon, Curr. Opin. Solid State Mater. Sci. **20**, 115 (2016).
[7] T. R. Anthony, J. Appl. Phys. **41**, 3969 (1970).
[8] T. R. Anthony, Acta Metall. **18**, 307 (1970).
[9] T. Kato, H. Takahashi, and M. Izumiya, J. Nucl. Mater. **189**, 167 (1992).
[10] J. Gan, E. Simonen, S. Bruemmer, L. Fournier, B. Sencer, and G. Was, J. Nucl. Mater. **325**, 94 (2004).
[11] M. Nastar, V. Y. Dobretsov, and G. Martin, Philos. Mag. A **80**, 155 (2000).
[12] M. Nastar, Philos. Mag. **85**, 3767 (2005).
[13] D. R. Trinkle, Philos. Mag. **97**, 2514 (2017).
[14] T. Garnier, V. R. Manga, D. R. Trinkle, M. Nastar, and P. Bellon, Phys. Rev. B **88**, 134108 (2013).
[15] T. Garnier, M. Nastar, P. Bellon, and D. R. Trinkle, Phys. Rev. B **88**, 134201 (2013).
[16] T. Garnier, D. R. Trinkle, M. Nastar, and P. Bellon, Phys. Rev. B **89**, 144202 (2014).
[17] M. Nastar, Phys. Rev. B **90**, 144101 (2014).
[18] L. Messina, M. Nastar, N. Sandberg, and P. Olsson, Phys. Rev. B **93**, 184302 (2016).
[19] T. Schuler and M. Nastar, Phys. Rev. B **93**, 224101 (2016).
[20] A. Claisse, T. Schuler, D. A. Lopes, and P. Olsson, Phys. Rev. B **94**, 174302 (2016).
[21] T. Schuler, D. A. Lopes, A. Claisse, and P. Olsson, Phys. Rev. B **95**, 094117 (2017).
[22] R. Agarwal and D. R. Trinkle, Phys. Rev. Lett. **118**, 105901 (2017).
[23] J.-L. Bocquet, C. Barouh, and C.-C. Fu, Phys. Rev. B **95**, 214108 (2017).
[24] A. Le Claire, in *Correlation Effects in Diffusion in Solids*, edited by W. Jost (Academic, New York, 1970), Chap. 5.
[25] A. Allnatt and A. Lidiard, *Atomic Transport in Solids* (Cambridge University Press, Cambridge, 2003).
[26] L.-J. Zhang, Z.-Y. Chen, Q.-M. Hu, and R. Yang, J. Alloys Compd. **740**, 156 (2018).
[27] X. Y. Liu and D. A. Andersson, J. Nucl. Mater. **498**, 373 (2018).
[28] H. Wang, X. Gao, H. Ren, S. Chen, and Z. Yao, J. Phys. Chem. Solids **112**, 153 (2018).
[29] W. Liu, N. Miao, L. Zhu, J. Zhou, and Z. Sun, Phys. Chem. Chem. Phys. **19**, 32404 (2017).
[30] C. D. Versteylen, N. H. van Dijk, and M. H. F. Sluiter, Phys. Rev. B **96**, 094105 (2017).
[31] D. Perez Daroca, Solid State Commun. **252**, 11 (2017).
[32] C. Barouh, T. Schuler, C.-C. Fu, and T. Jourdan, Phys. Rev. B **92**, 104102 (2015).
[33] E. Vathonne, D. A. Andersson, M. Freyss, R. Perriot, M. W. D. Cooper, C. R. Stanek, and M. Bertolus, Inorg. Chem. **56**, 125 (2017).
[34] D. Connétable, É. Andrieu, and D. Monceau, Comput. Mater. Sci. **101**, 77 (2015).
[35] A. B. Lidiard, London, Edinburgh, Dublin Philos. Mag., J. Sci. **46**, 1218 (1955).
[36] A. Le Claire, J. Nucl. Mater. **69-70**, 70 (1978).
[37] A. R. Allnatt, J. Phys. C: Solid State Phys. **14**, 5467 (1981).
[38] J. L. Bocquet, Philos. Mag. **94**, 3603 (2014).
[39] H. Wu, T. Mayeshiba, and D. Morgan, Sci. Data **3**, 160054 (2016).
[40] G. H. Vineyard, J. Phys. Chem. Solids **3**, 121 (1957).
[41] L. Onsager, Phys. Rev. **37**, 405 (1931).
[42] L. Onsager, Phys. Rev. **38**, 2265 (1931).
[43] H. H. Wu and D. R. Trinkle, Phys. Rev. Lett. **107**, 045504 (2011).
[44] R. Agarwal and D. R. Trinkle, Phys. Rev. B **94**, 054106 (2016).
[45] See Supplemental Material at http://link.aps.org/supplemental/10.1103/PhysRevMaterials.2.073605 for data point coordinates for Figs. 3, 4, and 5.
[46] M. Norgett, M. Robinson, and I. Torrens, Nucl. Eng. Des. **33**, 50 (1975).
[47] G. Was, *Fundamentals of Radiation Materials Science* (Springer, Berlin, 2007).
[48] R. S. Averback, R. Benedek, and K. L. Merkle, Phys. Rev. B **18**, 4156 (1978).
[49] P. Ehrhart and R. S. Averback, Philos. Mag. A **60**, 283 (1989).
[50] V. Naundorf, M.-P. Macht, and H. Wollenberger, J. Nucl. Mater. **186**, 227 (1992).
[51] R. Averback and T. D. D. L. Rubia, in *Solid State Physics*, Solid State Physics Vol. 51, edited by H. Ehrenreich and F. Spaepen (Academic, New York, 1998), pp. 281–402.
[52] M. Hackett, R. Najafabadi, and G. Was, J. Nucl. Mater. **389**, 279 (2009).
[53] F. Soisson and T. Jourdan, Acta Mater. **103**, 870 (2016).
[54] T. Schuler, C. Barouh, M. Nastar, and C.-C. Fu, Phys. Rev. Lett. **115**, 015501 (2015).